frontiers in Earth Science

ORIGINAL RESEARCH
published: 09 March 2022
doi: 10.3389/feart.2022.838299

# A Continuous 13.3-Ka Paleoseismic Record Constrains Major Earthquake Recurrence in the Longmen Shan Collision Zone

*Wei Shi*[1], *Hanchao Jiang*[1]*, *G. Ian Alsop*[2] *and Guo Wu*[3]

[1]State Key Laboratory of Earthquake Dynamics, Institute of Geology, China Earthquake Administration, Beijing, China, [2]Department of Geology and Geophysics, School of Geosciences, University of Aberdeen, Aberdeen, United Kingdom, [3]Institute of Geology, China Earthquake Administration, Beijing, China

Thrust collision zones with low slip rates along the plate boundary are significant areas of stress accumulation and prone to develop more destructive earthquakes with longer recurrence intervals. Such regions are often classified as low seismic risk if they lack continuous records of large earthquakes, such as the eastern Tibetan Plateau before the 2008 $M_w$ 7.9 Wenchuan earthquake. Here, we provide a continuous seismic record in the Longmen Shan thrust fault zone spanning 13,000 years based on detailed investigation of the soft-sediment deformation structures and seismites in the Lixian lacustrine sequence. The recurrence time of large earthquakes ($M \geq 8.1$) is 1,200 years, which is significantly shorter than the previous estimate of 2,000–6,000 years. The Maoxian-Wenchuan fault is the main fault that triggered the deformation in the Lixian lacustrine sediments. In addition, earthquake recurrence in the warm period is more frequent than that in the cold period, which should arouse our attention for the seismic study of tectonically active regions.

**Keywords: soft sediment deformation, seismites, major earthquake recurrence time, Longmen Shan fault zone, eastern Tibetan Plateau**

OPEN ACCESS

***Edited by:***
*Yuanyuan Fu,*
*China Earthquake Administration, China*

***Reviewed by:***
*Yueren Xu,*
*China Earthquake Administration, China*
*Ken Ikehara,*
*Geological Survey of Japan (AIST), Japan*
*Wenjun Zheng,*
*Sun Yat-sen University, China*

***Correspondence:**
*Hanchao Jiang*
*hcjiang@ies.ac.cn*

***Specialty section:***
*This article was submitted to Geohazards and Georisks, a section of the journal Frontiers in Earth Science*

***Received:*** *17 December 2021*
***Accepted:*** *14 February 2022*
***Published:*** *09 March 2022*

***Citation:***
*Shi W, Jiang H, Alsop GI and Wu G (2022) A Continuous 13.3-Ka Paleoseismic Record Constrains Major Earthquake Recurrence in the Longmen Shan Collision Zone. Front. Earth Sci. 10:838299. doi: 10.3389/feart.2022.838299*

## INTRODUCTION

Understanding fault behavior and assessing future seismic risks requires a foundation in instrumental, historical and palaeoseismic records (Berryman et al., 2012; Gomez et al., 2015; Scharer et al., 2010; Lu et al., 2020). According to a comprehensive analysis of historical and modern seismic data, no earthquake of $M \geq 7.0$ occurred in the Longmen Shan fault zone during at least 1,100–1,700 years before 2008 (**Figure 1**) (Wen et al., 2009). Moreover, the intensity of the 2008 $M_w$ 7.9 Wenchuan earthquake greatly exceeded the largest earthquake in the history of the Longmen Shan fault zone, indicating that it is far from sufficient to accurately assess the potential seismic risk of large active fault zones with low slip rates (**Supplementary Figure S1**) based on historical earthquake records from hundreds to thousands of years (Deng, 2008; Wen et al., 2009).

Previous studies infer that the recurrence interval of large earthquakes is 2,000–6,000 years in the Longmen Shan fault zone based on GPS and seismological slip rates (Zhang et al., 2008; Zhang, 2013; Ran et al., 2014). Large earthquakes usually have a long recurrence interval that can't be covered by instrumental and historical records. This makes it extremely important to get a long and continuous palaeoseismic record for assessing fault activities and future seismic risks.

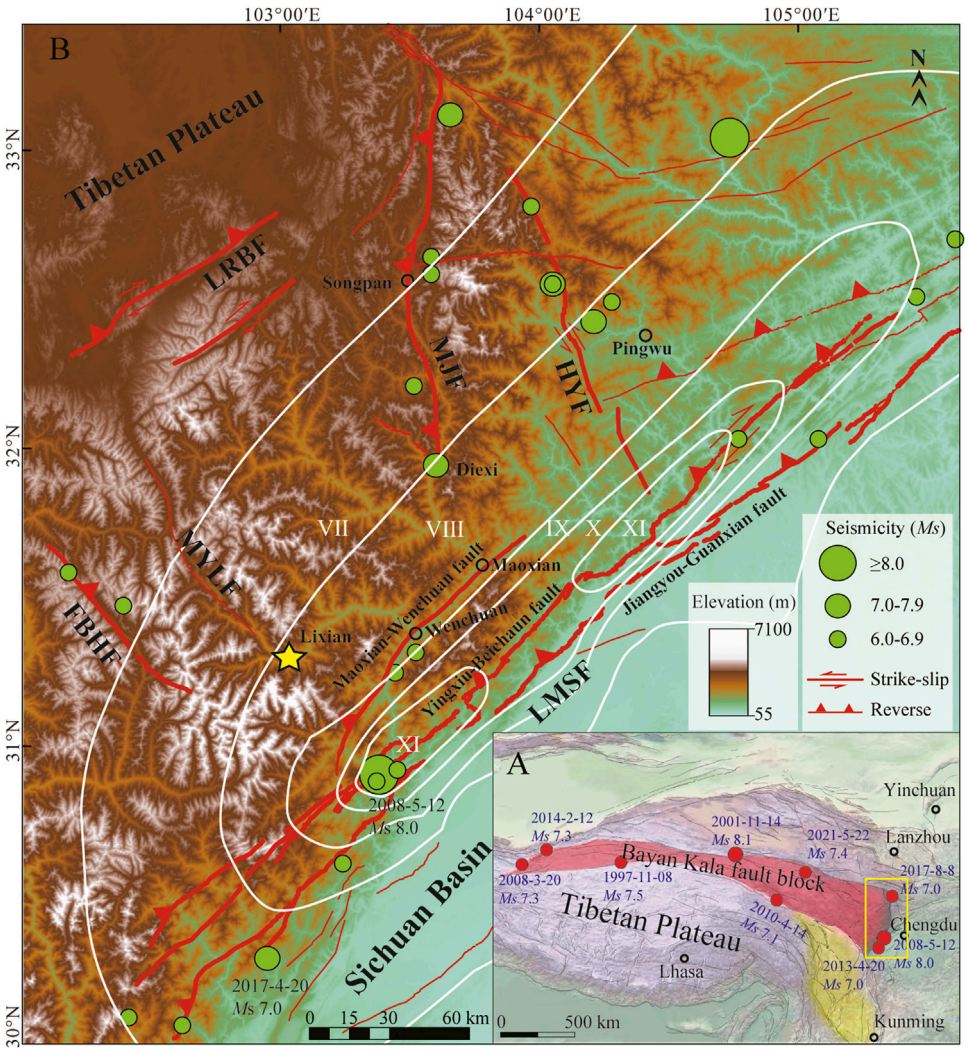


**FIGURE 1 |** Tectonic setting of the eastern margin of Tibetan Plateau **(A)** Epicenters distribution for $M_s \geq 7.0$ earthquakes in the Bayan Kala fault block since 1995 (Deng et al., 2014). Yellow box shows the extent of the B diagram **(B)** Major active faults (Xu et al., 2009) and the seismicity of the eastern margin of Tibetan Plateau. Seismicity data are from the China Earthquake Data Center (http://data.earthquake.cn/data). White line represents seismic intensity of Wenchuan earthquake. LMSF, Longmen Shan fault; LRBF, Longriba fault; HYF, Huya fault; MJF, Minjiang fault; MYLF, Miyaluo fault; FBHF, Fubianhe fault. The yellow star represents the Lixian section.

Paleoseismological trenching at suitable sites can extend the record for surface rupturing earthquakes to the past few thousand years (Moernaut, 2020), but continuity is not guaranteed. Lacustrine paleoseismology can capture long continuous records of strong seismic shaking, which integrate the activity of all significant seismic sources in a region and allow a reliable determination of recurrence patterns (Moernaut, et al., 2018; Ghazoui et al., 2019; Lu et al., 2020; Oswald et al., 2021), including soft-sediment deformation (SSD, co-seismic) and seismites (post-seismic). Among them, *in-situ* SSD structures can record a seismic event (Xu et al., 2015; Jiang et al., 2016; Lu et al., 2017, 2020; Zhong et al., 2019; Zhang et al., 2021; Fan et al., 2022). Some seismites overlay the SSD, others lack an underlying SSD but are temporally correlated with a historic earthquake (Lu et al., 2017).

In the eastern margin of the Tibetan Plateau, the geomorphological features of alpine valleys (**Supplementary Figure S1**) cause the serious absence of Quaternary sediments and thus paleoseismic records, which leads to poor research on the recurrence model of regional earthquakes. This brings severe challenges to the seismic risk assessment. Fortunately, the 13.3-ka-long continuous lacustrine sequence at Lixian (31.44°N, 103.16°E; 1867 ± 7 m a.s.l.) represents a precious chance to reveal palaeoseismic events, because previous studies have shown that the SSD structures and/or coarse-silt event layers in the lacustrine sediments in the tectonically active regions point to seismic genesis (Jiang et al., 2014, 2016, 2017; Liang and Jiang, 2017). However, there is a lack of quantitative analysis of event layers and seismic intensity in the eastern Tibetan Plateau.

In this study, our target is to link the SSD structures and/or seismites in the Lixian lacustrine sequence, which were published by Jiang et al. (2016, 2017), with the earthquake magnitude based on the existing fluid dynamics modeling. Recurrence mode of regional earthquakes and its controlling factors are addressed. This is of great scientific significance for assessment of the seismic risk in the tectonically active regions which are characterized by geomorphology of alpine valley and absence of Quaternary deposits.

## GEOGRAPHIC AND GEOLOGIC SETTINGS

The Longmen Shan fault zone extends ~500 km from NE to SW and is composed of three groups of oblique, high-angle, listric-reverse faults (**Figure 1B**, **Supplementary Figure S1**) (Zhang et al., 2010). It separates the Tibetan Plateau from the Sichuan Basin, making it the most significant geomorphologic gradient zone in China. GPS measurements produce a short-term slip-rate of 1–2 mm $yr^{-1}$ (**Supplementary Figure S1**) (Zhang et al., 2010), which is consistent with the long-term denudation rates by thermochronology analysis of zircon and apatite during the Late Cenozoic (Kirby et al., 2002).

Since the beginning of the 21st century, the major earthquakes in inland China are mainly distributed around the Bayan Kala block (**Figure 1A**), indicating that it is currently the main active block of strong earthquakes (Deng et al., 2010, 2014), and shows signs of gradually migrating towards the east. The 2008 Wenchuan *M*w 7.9 earthquake occurred on the Longmen Shan fault zone, the easternmost margin of the Bayan Kala block, and triggered surface rupture of 240 km on Yingxiu-Beichuan fault and 72 km on Pengxian-Guanxian fault (Xu et al., 2009), and >56, 000 landslides, covering a total area of >396 $km^2$ (Dai et al., 2011; Li et al., 2014; Xu et al., 2014). This brings severe challenges to the seismic risk assessment in the eastern margin of the Tibetan Plateau.

The geomorphological features of alpine valleys characterize the eastern margin of the Tibetan Plateau, which leads to less preservation of the Quaternary sediments. Instead, Paleozoic to Mesozoic bedrock outcrop widely. The bedrock is mainly composed of Silurian phyllite, quartz schist, Triassic phyllite, metamorphic sandstone and the Neoproterozoic Pengguan complex in the middle section of Longmen Shan fault zone.

The study area is poorly covered by vegetation and dominated by a windy and semi-arid climate (Shi et al., 2020; Xu et al., 2020; Wei et al., 2021). The high wind speeds occur in April (average 4.9 m/s) while the low ones occur in July (average 3.7 m/s). The highest instantaneous wind speed can reach 21 m/s (Liu, 2014). The mean annual precipitation (MAP) ranges from 500 to 850 mm, and 75% of the precipitation falls in the rainy seasons of May to October (Ding et al., 2014). Such a windy and semi-arid climate is apt for widespread transport of dust particles, given that moderate to strong earthquakes usually generate dust storms (Jiang et al., 2017).

## MATERIALS AND METHODS

### Earthquake Indicators and Paleoseismic Events

Linking SSD structures with earthquakes is commonly based in tectonically active areas, deformation of fine grained material, vertical repeatability, lateral traceability, separation by non-deformed layers, occurrence of SSD types simulated in laboratory, and exclusion of gravity collapse (Sims, 1975; Owen and Moretti, 2011; Jiang et al., 2016). According to these six criteria, seismic events can be recognized from SSD structures in the lacustrine sediments. Intriguingly, the SSD layers are always covered by coarse-silt layers in the Lixian sequence (Jiang et al., 2017). Based on the sedimentological analysis of high-resolution grain-size proxies, such as end-member analysis, C-M (C: one percentile, M: median diameter) diagram, Sahu value (Sahu, 1964), and so on, these layers are caused by earthquakes that triggered dust storms and massive landslides and then changed the source of dust particles (**Figure 3**) (Jiang et al., 2017). As a result, the Lixian section displays a much higher deposition rate of 1.75 mm/yr than that of the southern Chinese Loess Plateau (~0.08 mm/yr, Ding et al., 1994). This analysis is corroborated by continuously fine-grained (mean grain size: 15.9 μm) deposition at the Lixian lakeshore instead of coarse-grained sediments usually caused by fluvial flow (**Supplementary Figure S2**). Therefore, SSD structures and coarse-silt layers are used as sedimentological indicators of seismic events (Jiang et al., 2016, 2017).

Seismic shaking with different intensity can trigger the different types of SSD structures of the water-saturated sediments, and the stronger earthquakes usually result in stronger deformation (Rodrı´guez-Pascua et al., 2000; Wetzler et al., 2010; Lu et al., 2020). Accordingly, SSD of similar types in different regions probably correspond to the same triggering mechanism and intensity conditions. On this basis, fluid dynamics modeling is used to obtain the peak ground acceleration (PGA) required to trigger the typical types of deformation (Wetzler et al., 2010; Lu et al., 2020).

### Peak Ground Acceleration

Previous studies indicate that earthquakes with different intensity can lead to different types of SSD structures, and the fluid dynamics modeling are used to obtain the PGA required to trigger different types of SSD structure (Wetzler et al., 2010; Lu et al., 2020). The lower-bounding magnitude of SSD is *M*w ≥ 5.3 with PGA ≥0.13 g Modified Mercalli Intensity (MMI) ≥ VI½ in the Dead Sea (Lu et al., 2020).

In this study, we collectively analyzed the SSDs in the Lixian section. The clastic dyke and micro-faults are cross-layer and often occur locally in the strata (Jiang et al., 2016), so continuity is not guaranteed, and the age is uncertain. The clastic gravel in Lixian section is composed of bedrock debris, which is possibly triggered by bedrock landslides induced by earthquakes of different intensity (Jiang et al., 2016). We eliminate these SSDs in the whole Lixian sequence. In

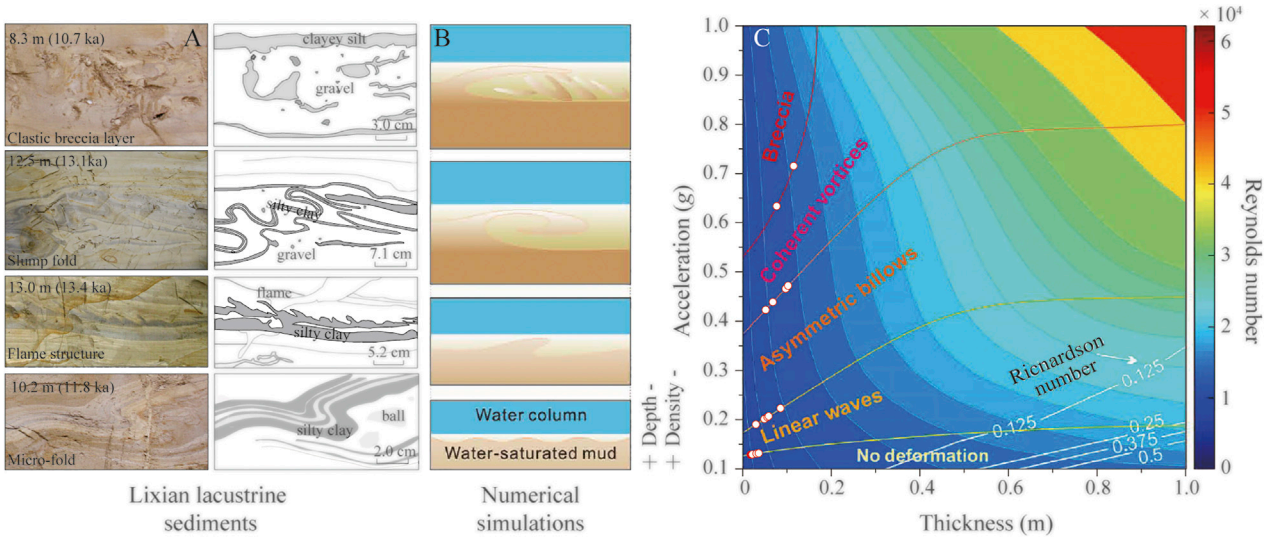


**FIGURE 2 |** SSD structures in the Lixian lacustrine sequence and the numerical simulation **(A)** Typical structures from the Lixian section outcrops (jiang et al., 2016) **(B)** Schematic diagrams of the four structures from the numerical simulations (Lu et al., 2020) **(C)** Quantitative estimation of the accelerations that are needed to initiate the four structures with different thicknesses (Lu et al., 2020). The circle represents different thickness and types of SSD in the Lixian section.

addition, ball-and-pillow structure in Jiang et al. (2016) are named according to deformation patterns, which cannot clearly reflect the strength of the deformation. Corresponding to the fluid dynamics modeling, the ball-and-pillow structures exhibit minimal deformation, so we redefined them as "micro-folds". The micro-folds can reflect the initial stage of the flame structures and slump folds (Jiang et al., 2016). As the deformation continues to intensify, clastic breccia layers are formed when the original rock strata break up.

As mentioned above, four typical types of SSDs, i.e. micro-folds, flame structures, slump folds and clastic breccia layers are identified corresponding to linear waves, asymmetric billows, coherent vortices and intraclast breccia layer, respectively (**Figure 2A,B**) (Jiang et al., 2016; Lu et al., 2020). We project the different types and thicknesses of SSD into the acceleration-thickness diagram to get the PGAs required to trigger different types of SSD in the Lixian section.

## PGA- MMI Relations

The degree of ground shaking during earthquakes can be determined by the documented PGA and MMI (Bilal and Askan, 2014). In various earthquake studies, MMI is inferred from regional datasets, peak ground-motion data, isoseismic maps, and earthquake damage reports (Worden et al., 2012), especially in paleoseismic studies. Du et al. (2019) established the relationship between MMI and PGA in the Longmen Shan fault zone based on 34 moderate to large earthquakes. In this study, we use this relationship to infer the MMI information of the paleoseismic records in the Lixian section.

The equation is expressed as

$$\mathrm{MMI} = 3.311 \log \mathrm{PGA} - 0.354 \quad (1)$$

## Intensity (I) - Magnitude (*M*) - Epicentral Distance (R) Relations

Establishing a seismic attenuation relationship is an important action in regional evaluation of seismic risk (Lei et al., 2007). Due to the complex tectonic background in China, there are significant differences in seismic attenuation relationships established in different regions.

Lei et al. (2007) established a seismic attenuation relationship based on 96 recent destructive earthquakes in Southwest China as follows.

$$\text{Long axis}: \ I_a = 7.3568 + 1.2780M - 5.0655lg(R_a + 24) \quad (2)$$

$$\text{Short axis}: \ I_b = 3.9502 + 1.2780M - 3.7567g(R_b + 9) \quad (3)$$

where I is the intensity of the MMI and R is the epicentral distance.

Considering that the Wenchuan earthquake intensity isoseismal map is distributed along the strike of the Longmen Shan fault zone (NE-SW), and the Lixian section is located on its short axis (**Figure 1B**). In this study, we use the short-axis relationship to study the seismic record of the Lixian section.

## B Value and Completeness of Magnitude

The b value is the most important parameter in the magnitude-frequency relationship (Gutenberg-Richter distributions) (Wesnousky, 1995), and plays an important role in seismicity studies and seismic hazard analysis. In order to obtain a reliable complete earthquake catalog and b value, we use the empirical relations (Lei et al., 2007; Du et al., 2019) to obtain the fault distribution range and epicenter distance that triggered the lowest-degree deformation in the Lixian section based on the upper limit of potential source earthquake. We extract the seismic

data (6,435 data from 1970 to 2020) within the range of 95 km away from the Lixian section.

The minimum completeness magnitude (*Mc*) is identified by the methods of cumulative number of earthquakes plotted against time and maximum curvature (Woessner and Wiemer, 2005). On this basis, the maximum likelihood method is used to fit the corresponding seismicity parameters (b value).

# RESULTS

## Magnitude Constraint for SSD

In the Lixian section, we identified 17 SSD layers (**Supplementary Table S1**). Due to the absence of paleoseismic records from the middle Holocene (~6.0 ka) to present in the Lixian section, the 2008 $M_w$ 7.9 Wenchuan earthquake provided a favorable condition for the magnitude limitation of large earthquakes in this study. Analysis of empirical equation and inversion suggests that the instrumental data (PGA = 0.21–0.38, Liu and Li, 2009) around the Lixian section correspond to the magnitudes of 7.9–8.5 and MMI of Ⅶ–Ⅷ of the Wenchuan earthquake, by taking R = 50 km (epicentral distance). The above results are consistent with the actual data ($M_w$ of 7.9, MMI of Ⅷ–Ⅸ). These results increase the reliability of the empirical equation applied in the eastern margin of the Tibetan Plateau.

In this study, six layers of micro-folds, five layers of flame structures, four layers of slump folds and two layers of clastic breccia have been identified in the Lixian lacustrine sequence (**Supplementary Table S1**, **Figure 2A**). According to the distribution of different types of the Lixian SSD strcutures in the acceleration-thickness diagram (**Figure 2C**), the PGA for triggering SSD is ≥0.13g, ≥ 0.19g, ≥ 0.43 g and ≥0.63 g (**Supplementary Table S2**). Because the projection points are on the boundary of different deformation types, we obtained the lower boundary of acceleration that can reflect the triggering of typical deformation on the eastern margin of the Tibetan Plateau. According to the regional empirical equation (Du et al., 2019), we constrain the intensity of the four typies of SSD paleoearthquake records with MMI ≥ Ⅵ½, ≥ Ⅶ, ≥ Ⅷ½ and ≥ Ⅸ (**Supplementary Table S2**).

According to the regional empirical attenuation relations and regional geological survey, the middle segment of Longmen Shan fault zone is the main fault that triggered deformations in the Lixian lacustrine sequence, while the Miyaluo fault can only trigger the low-degree deformations (micro-folds and flame structures) (**Supplementary Text S1**). In this study, the minimum epicentral distance triggering deformation in the Lixian section is limited to $R_{min} \geq 10$, and the $R_{max} \leq 95$ km (**Supplementary Table S3**). According to the regional empirical equation (Lei et al., 2007; Du et al., 2019), the six layers of micro-folds (MMI ≥ Ⅵ½, PGA ≥0.13) and five layers of flame structures (MMI ≥ Ⅶ, PGA ≥0.19) recorded in the Lixian lacustrine sequence correspond to magnitudes of $M \geq 5.9$, 6.3 ($R_{min} \geq$ 10 km) and $M \geq 6.8$, 7.2 ($R \geq 30$ km), respectively (**Table 1**). Previous studies show that SSD can be triggered by $M_w > 5.7$ in or near isoseismic lines with MMI ≥ VII (Monecke et al., 2006). Multiple faults in the region considered are likely to trigger low-degree deformations in the Lixian lacustrine sequence. Therefore, MMI ≥ Ⅵ½ ($M \geq 5.9$) are taken as the lower-boundary conditions for triggering the deformation in the Lixian lacustrine sequence, by taking $R_{min} \geq 10$ km.

Four layers of slump folds (MMI ≥ Ⅷ½) and two layers of clastic breccia layers (MMI ≥ Ⅸ) recorded in the Lixian section correspond to PGA of 0.43 and 0.63, respectively, which are probably a response to the larger seismic shaking in the middle segment of the Longmen Shan fault zone. According to the regional empirical equation (Lei et al., 2007; Du et al., 2019), the MMI ≥ Ⅷ½ and Ⅸ earthquake events correspond to $M \geq 8.1$ and 8.6, by taking $R_{min} \geq 30$, respectively (**Table 1**). The trigger conditions for slump folds ($M \geq 8.1$, MMI ≥ Ⅷ½) are consistent with the actual data of the Wenchuan earthquake ($M_w$ of 7.9, MMI of Ⅷ - Ⅸ), which well constrain the largest earthquake magnitude of the Lixian section. Because only two layers of clastic breccia are recorded in the Lixian lacustrine sequence which are less representative (**Figure 2C**), and the $M \geq 8.6$ is much larger than the potential source magnitude ($M$ = 8.0) in the eastern margin of the Tibetan Plateau (**Supplementary Figure S3**), the clastic breccia layers in this study are divided into slump folds. Thus, $M \geq 8.1$ is the highest magnitude recorded by SSD structures in the Lixian lacustrine sequence.

## Magnitude Constraint for Coarse-Silt Layers

Besides the SSD layers in the study area, there are also many coarse-silt layers, among which 17 directly overlie the SSD layers, indicating that deformation developed at the sediment surface (e.g. Alsop et al., 2022) (**Figure 4A**) and 46 layers exist independently (**Figure 4B**, **Supplementary Table S4**). These coarse-silt layers are caused by earthquakes, through which many more sources of clastic particles increased instantly and supplied plenty of dust particles for the study area (**Figure 3**) (Jiang et al., 2017). Generally, the thickness of the seismic event layers recorded by lacustrine sediments can be correlated with the seismic intensity, and further used to infer the regional palaeoseismic intensity (Moernaut et al., 2014).

The SSD thickness in the Lixian section has a good correlation (coefficient of 0.67) with seismic intensity, while the correlation weakens between thickness of coarse-silt layers that overlie SSD and seismic intensity with a low coefficient of 0.30 (**Figure 4C,D**). Intriguingly, when MMI is ≤ Ⅵ½, the thickness of coarse-silt layers are less than 10 cm (**Figure 4D**); when MMI is > Ⅵ½, the coarse-silt layers become thicker with the increase of intensity. The thickest is up to 19 cm (MMI ≥ Ⅷ½). Therefore, the thickness ≥19 cm of coarse-silt layer is linked with MMI ≥ Ⅷ½ event, and the 10–19 cm layer is linked with MMI ≥ Ⅶ event in this study.

In addition, the China seismic intensity scale shows that MMI of Ⅵ can produce slight damage, and MMI ≥ Ⅶ is a destructive earthquake (http://www.gb688.cn/bzgk/gb/index). The boundary condition for deformation of linear waves in the Lixian section is MMI ≥ Ⅵ½ (PGA ≥0.13 g), which is sufficient to produce geomorphic destruction. Therefore, 35 event layers of coarse

**TABLE 1 |** Magnitude constraint for paleosesmic events in the Lixian section.

| Epicentral distance (R; to Lixian, km) | Earthquake indicators | Acceleration[a] (*g*) | Intensity[b] (MMI) | Magnitude[c] ($M_{min}$) |
|---|---|---|---|---|
| ≥10 | Micro-folds | ≥0.13 | ≥ VI½ | ≥5.9 |
| | Flame structures | ≥0.19 | ≥ VII | ≥6.3 |
| ≥30 | Micro-folds | ≥0.13 | ≥ VI½ | ≥6.8 |
| | Flame structures | ≥0.19 | ≥ VII | ≥7.2 |
| | Slump folds | ≥0.43 | ≥ VIII½ | ≥8.1 |
| | Clastic breccia layers | ≥0.63 | ≥ IX | ≥8.6 |

[a]*Data are obtained from* ***Supplementary Figure S4C****.*
[b]*Based on MMI, 3.311 log PGA, 0.354 (Du et al., 2019).*
[c]*Based on* $I_b$ = 3.9502 + 1.2780*M* - 3.7567 g ($R_b$ + 9) *(Lei et al., 2007).*

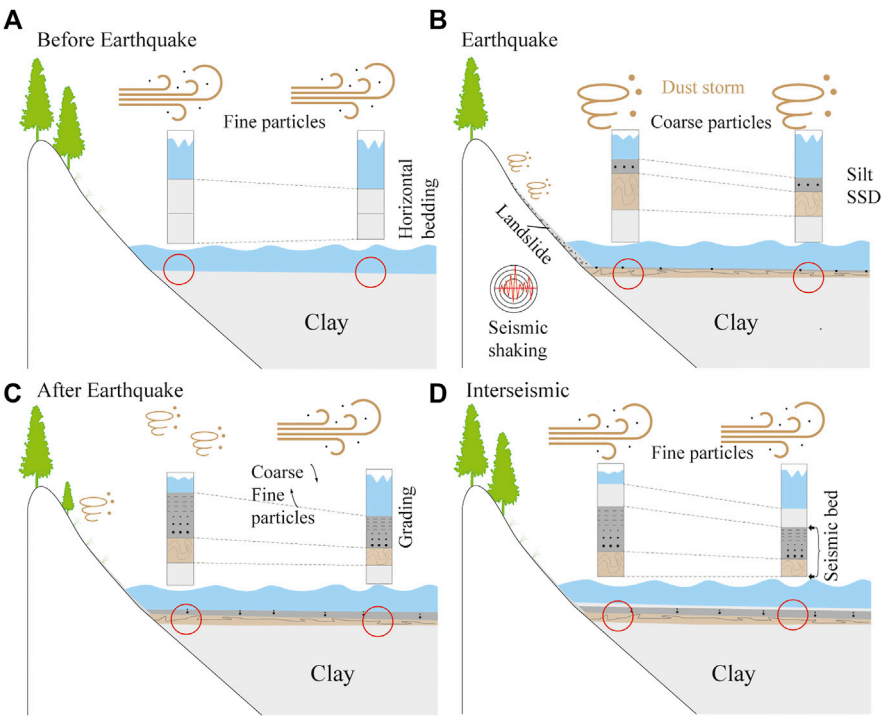


**FIGURE 3 |** Conceptual model of seismic layers **(A)** Background dust deposition before earthquake, with horizontal bedding **(B)** The earthquake shaking not only causes deformation of the water-saturated sediments but also provides abundant fresh coarse particles through dust storms, large quantities of landslides and surface loosening **(C)** As the landscape and vegetation restore, coarse particles decrease while fine particles increase **(D)** The source of lake sediments restores to its pre-earthquake level, and a seismic event layer is recorded.

particles (5–10 cm) occurring independently correspond probably to the moderate-strong earthquakes with MMI ≥ VI½.

# DISCUSSION

## A 13.3-Ka-Long Earthquake Record

Considering that the aftershocks of the 2008 Wenchuan earthquake are too many to represent the long-term seismic activity in the study area, the space-time window method (Gardner and Knopoff, 1974) is used to delete the fore- and aftershocks. Based on the analysis of seismic data from 1970 to 2020 (**Supplementary Figure S4A**), the quality of seismic records after 1986 (**Supplementary Figure S4B**) is high with $M_c$ of 3.5 and b value of 1.06 (**Figure 5F**).

The frequency-magnitude relationship shows that the moderate-strong earthquakes ($M \geq 5.9$) and the strong earthquakes ($M \geq 6.3$) records in the Lixian section extends the fitting line of Gutenberg-Richter relationship from 5.3 to 6.3 with b value of 1.06 (**Figure 5F**), which indicates that the palaeoseismic records revealed by this study make up for the vacancy of the regional moderate-strong earthquakes and increase their completeness. The large earthquakes ($M \geq 8.1$) are much more frequent than in the fitting line of Gutenberg-Richter relationship (**Figure 5F**), which possibly indicate regional characteristic

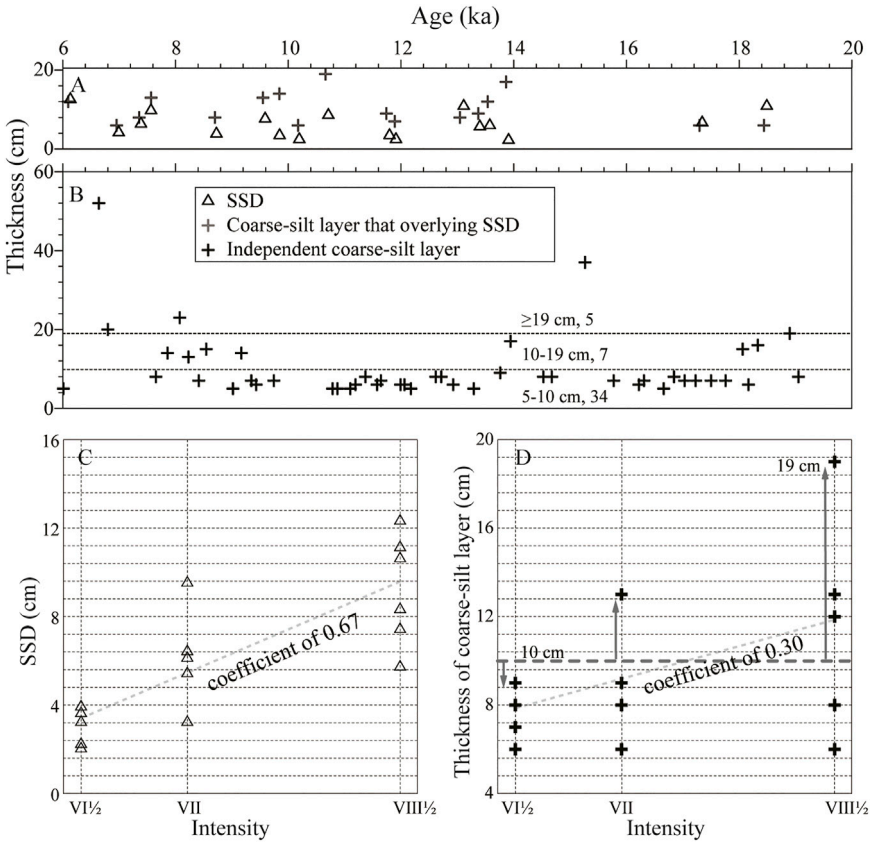


**FIGURE 4 |** Thickness variations and analysis of the SSD structures and coarse-silt layers with time **(A)** Distribution characteristics of the SSD structures and overlying coarse-silt layers, and **(B)** the independent coarse-silt layers **(C)** Correlation of SSD structure and **(D)** its overlying coarse-silt layers with MMI, note that the SSD thickness has better correlation with seismic intensity that than its overlying coarse-silt layers.

earthquakes (Wesnousky, 1995). Nevertheless, the significantly low b values (0.5–1.2) in Mianzhu-Maoxian of the middle-north segment of the Longmen Shan fault zone reflect the sliding state of frequent moderate-small earthquakes under the relatively high stress (Yi et al., 2006; Yi et al., 2008; Yang and Zhang, 2010), and strong earthquakes are most likely to occur in the future. This is consistent with many strong earthquakes in the middle segment of Longmen Shan fault zone revealed by this study, which implies that the magnitude constraint for strong seismic shaking events in this study is appropriate.

## Earthquake Recurrence Models and Trigger Mechanism

Linear interpolation was carried out based on the existing optically stimulated luminescence (OSL) dating results (**Supplementary Figure S5**, Jiang et al., 2016) to define the timing of paleoseismic events in the Lixian section. The 63 moderate-strong earthquakes of MMI ≥ VI½ ($M \geq 5.9$) in the Lixian lacustrine record have a mean recurring time of 210 years (**Figure 5A** and **Table 2**). The mean recurring time of strong earthquakes of MMI ≥ VII ($M \geq 6.3$) is about 600 years. The large earthquakes of MMI ≥ VIII½ ($M \geq 8.1$) have the longest recurring time of 1,200 years.

The dimensionless coefficient of variation (COV) is a commonly used parameter in describing earthquake recurrence model, which includes "quasi-periodic" (COV ≤0.7), random (COV ≈1) and "clustered" (aperiodic, COV >1) (Kagan and Jackson, 1991; Berryman et al., 2012; Griffin et al., 2020; Moernaut, 2020). For intraplate settings, a Poisson or clustered recurrence model seems the most appropriate, while plate boundaries generally show quasi-periodic or weakly periodic of recurrence intervals (Williams et al., 2019; Moernaut, 2020). The MMI ≥ VI½, ≥ VII and ≥ VIII½ events recorded in the Lixian section have the COV of 0.66, 1.06, 0.77, respectively (**Table 2**; **Figure 5**). In the following, we discuss the recurrence models and trigger mechanism of these three types earthquake.

The Longmen Shan fault zone is developed along the eastern margin of the Tibetan Plateau, which is the plate boundary between the Bayan Kala fault block and Sichuan Basin (**Figure 1**). It has a low slip rate (**Supplementary Figure S1**) (Zhang, 2013). The recurrence interval of the 13.3-ka-long large earthquake records of MMI ≥ VIII½ ($M \geq 8.1$) follows the Weibull distribution (**Figure 5**) with a small COV (0.77), which reflects the weak quasi-periodic recurrent model of the plate boundary

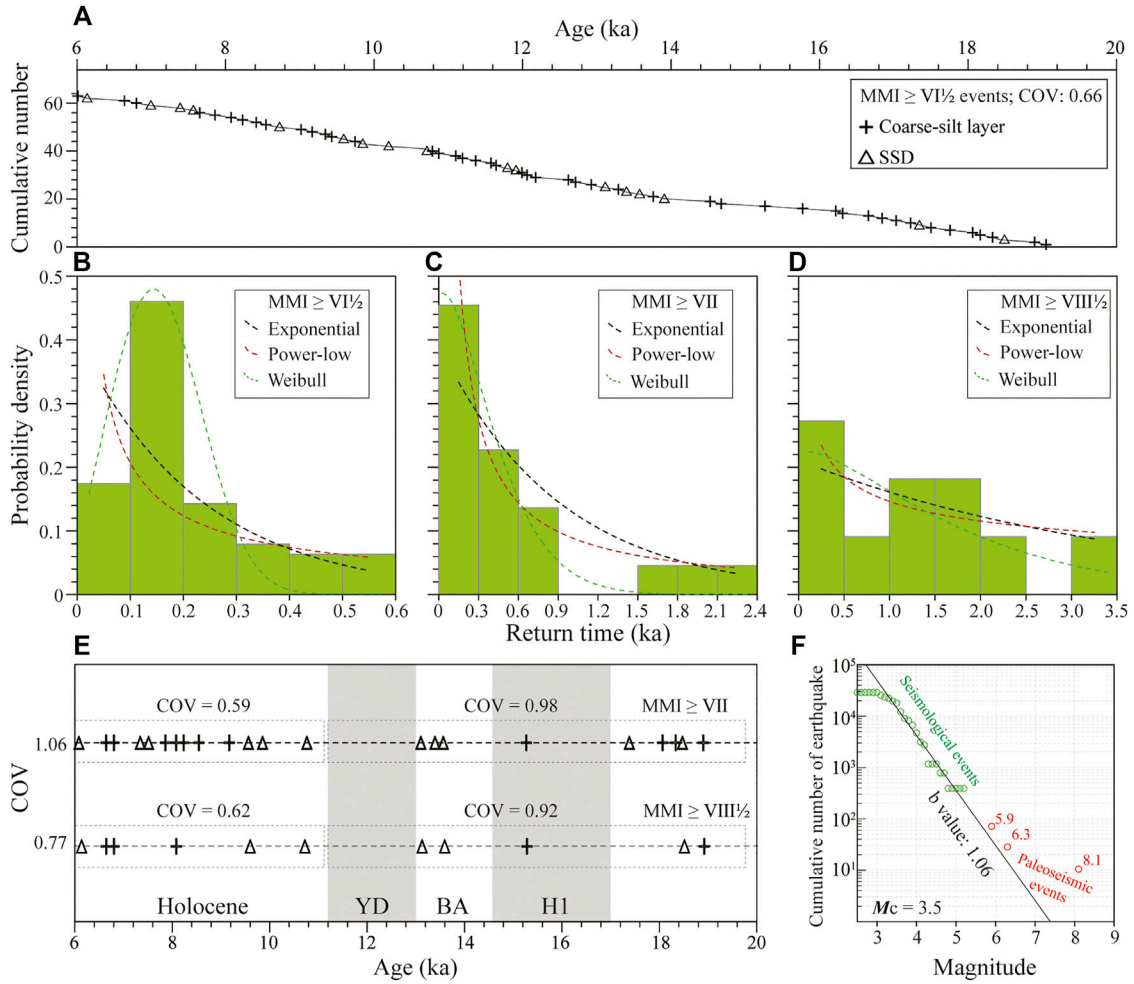


**FIGURE 5 |** Recurrence time statistics of seismites and magnitude constraint for strong seismic shaking events during 6.0–19.3 ka **(A)** Temporal distribution of moderate (MMI ≥ VI½) seismic shaking events **(B–D)** Histograms for return times of MMI ≥ VI½, ≥ VII, and ≥ VIII½ events. We plot difference distribution types (exponential, power-law and Weibull) for each dataset **(E)** Temporal distributions of strong and large earthquakes of the Lixian section **(F)** Magnitude-frequency distribution of modern (green colored) and paleoseismic (red colored) of the Lixian section during 6.0–19.3 ka.

**TABLE 2 |** Statistical analysis of recurrence times for the referred records.

| | | **MMI ≥ VI½ events** | **MMI ≥ VII events** | **MMI ≥ VIII½ events** |
|---|---|---|---|---|
| Magnitude (*M*) | | ≥5.9 | ≥6.3 | ≥8.1 |
| PGA | | ≥0.13 g | ≥0.18 g | ≥0.43 g |
| Time period | | 6.0–19.3 ka | 6.0–19.3 ka | 6.0–19.3 ka |
| Number of events | | 63 | 22 | 11 |
| Mean recurrence time (year) | | 210 | 600 | 1,200 |
| COV | | 0.66 | 1.06 | 0.77 |
| Fitting of return time distribution ($R^2$) | Weibull | 0.82 | 0.95 | 0.48 |
| | Exponential | 0.76 | 0.92 | 0.38 |
| | Power-law | 0.57 | 0.98 | 0.41 |
| Earthquake recurrence model | | quasi-periodic | random | quasi-periodic |

(Williams et al., 2019; Moernaut, 2020). The 1,200 years of recurrence interval of large earthquakes in the Lixian section is much shorter than 2,000–6,000 years inferred previously (Zhang et al., 2008; Zhang, 2013; Ran et al., 2014), which indicates the continuous lacustrine sequence are of great scientific significance in revealing a continuous paleoseismic record and assessing the seismic risk. The 2008 $M_w$ 7.9 Wenchuan earthquake occurred in the middle segment of Longmen Shan fault zone, which is the

seismogenic fault that possibly triggered the high-degree deformations in the Lixian lacustrine sequence. In addition, the isolated and geometrically simple plate boundary faults exhibit relatively regular recurrence patterns (quasi-periodic) (Berryman et al., 2012). Therefore, the weak quasi-periodic recurrent model of large earthquakes recorded in the Lixian section may respond to the periodic accumulation and release of energy in the Longmen Shan fault zone caused by the mutual compression of the Tibetan Plateau and South China block (Zhang et al., 2003). In contrast, the MMI ≥ VI½ ($M \geq 5.9$) earthquake records also show the stronger quasi-periodic (the Weibull distribution and COV of 0.66) (**Figure 5**), which may be due to the combined effect of multiple faults (Longmen Shan fault zone, Minjiang fault and Miyaluo fault, **Supplementary Figure S4**) leading to more frequent seismic records (**Supplementary Text S1**).

The MMI ≥ VII ($M \geq 6.3$) earthquake records follow a power-law distribution with a COV of 1.06, which indicate a random (Poisson) recurrence model in the in-plate (Williams et al., 2019; Moernaut, 2020). The additive influence of different active seismic sources can result in an overall Poisson recurrence process (Gomez et al., 2015), and the strong stress interactions on the complex fault geometry and other active faults in the vicinity can lead to irregular seismic cycles (Visini and Pace, 2014). Therefore, the random recurrence model of 13.3-ka-long earthquake events of MMI ≥ VII ($M \geq 6.3$) is a superposition response to the multiple active seismic sources of the middle segment of Longmen Shan fault zone and Miyaluo fault (**Supplementary Text S1**).

The number of MMI ≥ VII ($M \geq 6.3$) and MMI ≥ VIII½ ($M \geq 8.1$) earthquakes recorded in the Lixian section during the last deglaciation (11.6–18.0 ka) is significantly less than that in the early Holocene (6.0–11.6 ka). The most critical aspect is that only one earthquake is recorded during the Younger Dryas (YD, 11.6–12.9 ka) and Heinrich 1 (H1, 14.6–17.8 ka) (**Figure 5E**). Entering the Holocene, the number of earthquakes in the Lixian section increases significantly (**Figure 5**) and shows a "quasi-periodic" earthquake recurrence model (COV of 0.59 and 0.62), while a random recurrence model fits for the last deglaciation (COV of 0.98 and 0.92). The frequency of earthquake recurrence in Bølling-Allerød (BA) and Holocene (warm period) is more frequent, but much less in YD and H1 (cold period), which reflects the obvious correlation between earthquake occurrence and climate change in the Longmen Shan fault zone. This is comparable with the behavior of strong earthquakes ($M > 7$) in Japan, more frequent in spring and summer (warm) than in autumn and winter (cold) (Heki, 2003). The increase in pore-fluid pressure caused by groundwater recharge can trigger seismic activity by reducing the effective normal stress on the fault (Heki, 2003; Christiansen et al., 2005; Montgomery-Brown et al., 2019), and is deserving of further investigation in the future.

## CONCLUSION

We attempt to correlate the soft sediment deformation and seismic records in Lixian lacustrine sediments with earthquake intensity to discuss recurrence interval and recurrence models of regional paleoseismic events. We find that the MMI ≥ VI½ ($M \geq 5.9$, $R_{min} \geq 10$ km) is the lower-boundary condition for triggering deformation in the Lixian lacustrine sediments. The clastic breccia layer corresponds to the maximum earthquake magnitude ($M \geq 8.1$, MMI ≥ VIII½) recorded in the Lixian section. The recurrence time of large earthquakes ($M \geq 8.1$) is 1,200 years in the Longmen Shan collision zone. The Maoxian-Wenchuan fault is the main fault that triggered the slump folds and clastic breccia layers in the Lixian lacustrine sediments. In addition, the frequency of large earthquake recurrence in the warm period is more frequent than that in the cold period.

## DATA AVAILABILITY STATEMENT

The original contributions presented in the study are included in the article/**Supplementary Material**, further inquiries can be directed to the corresponding author.

## AUTHOR CONTRIBUTIONS

WS: Conceptualization, Methodology, Validation, Formal analysis, Investigation, Data Curation, Writing-Original Draft, Writing-Review and Editing, Visualization. HJ: Methodology, Investigation, Resources, Writing-Review and Editing, Project administration, Funding acquisition. GA: Writing- Review and Editing. GW: Methodology, Investigation.

## FUNDING

This study is supported by the National Nonprofit Fundamental Research of China Institute of Geology China Earthquake Administration (IGCEA 2126, 1906), the National Natural Science Foundation of China (41572346).

## SUPPLEMENTARY MATERIAL

The Supplementary Material for this article can be found online at: https://www.frontiersin.org/articles/10.3389/feart.2022.838299/full#supplementary-material

## REFERENCES

Alsop, G. I., Marco, S., and Levi, T. (2022). Recognising Surface Versus Sub-Surface Deformation of Soft-Sediments: Consequences and Considerations for Palaeoseismic Studies. *J. Struct. Geol.* 154, 104493. doi:10.1016/j.jsg.2021.104493

Berryman, K. R., Cochran, U. A., Clark, K. J., Biasi, G. P., Langridge, R. M., and Villamor, P. (2012). Major Earthquakes Occur Regularly on an Isolated Plate Boundary Fault. *Science* 336 (6089), 1690–1693. doi:10.1126/science.1218959

Bilal, M., and Askan, A. (2014). Relationships between Felt Intensity and Recorded Ground-Motion Parameters for Turkey. *Bull. Seismol. Soc. Am.* 104 (1), 484–496. doi:10.1785/0120130093

Christiansen, L., Hurwitz, S., Saar, M., Ingebritsen, S., and Hsieh, P. (2005). Seasonal Seismicity at Western United States Volcanic Centers. *Earth Planet. Sci. Lett.* 240 (2), 307–321. doi:10.1016/j.epsl.2005.09.012

Dai, F. C., Xu, C., Yao, X., Xu, L., Tu, X. B., and Gong, Q. M. (2011). Spatial Distribution of Landslides Triggered by the 2008 $M_s$ 8.0 Wenchuan Earthquake, China. *J. Asian Earth Sci.* 40 (4), 883–895. doi:10.1016/j.jseaes.2010.04.010

Deng, Q. D., Gao, X., Chen, G. H., and Yang, H. (2010). Recent Tectonic Activity of Bayan Kala Fault-Block and the Kunlun-Wenchuan Earthquake Series of the Tibetan Plateau. *Earth Sci. Front.* 17 (5), 163–178. in Chinese. CN/Y2010/V17/I5/163

Deng, Q. D., Cheng, S. P., Ma, J., and Du, P. (2014). Seismic Activities and Earthquake Potential in the Tibetan Plateau. *Chin. J. Geophys.* 57 (5), 2025–2042. in Chinese. doi:10.6038/cjg20140701

Deng, Q. D. (2008). Some Thoughts on the $M_s$ 8.0 Wenchuan, Sichuan Earthquake. *Seismol. Geol.* 30 (4), 811–827. in Chinese. doi:10.3969/j.issn.0253-4967.2008.04.001

Ding, Z., Yu, Z., Rutter, N. W., and Liu, T. (1994). Towards an Orbital Time Scale for Chinese Loess Deposits. *Quat. Sci. Rev.* 13 (1), 39–70. doi:10.1016/0277-3791(94)90124-4

Ding, H. R., Ma, G. W., Ni, S. J., Shi, Z. M., Zhao, G. H., Yan, L., et al. (2014). Study on Sediment Discharge Increase Caused by Wenchuan Earthquake Landslide and Heavy Rainfall in the Upper Reaches of the Min River. *J. Sichuan Univ.* 46 (3), 49–55. in Chinese. doi:10.15961/j.jsuese.2014.03.006

Du, K., Ding, B., Luo, H., and Sun, J. (2019). Relationship between Peak Ground Acceleration, Peak Ground Velocity, and Macroseismic Intensity in Western China. *Bull. Seismol. Soc. Am.* 109 (1), 284–297. doi:10.1785/0120180216

Fan, J. W., Xu, H. Y., Shi, W., Guo, Q. Q., Zhang, S. Q., Wei, X. T., et al. (2022). A ~28-kyr Continuous Lacustrine Paleoseismic Record of the Intraplate, Slow-Slipping Fuyun Fault in Northwest China. *Front. Earth Sci.* 10, 828801. doi:10.3389/feart.2022.828801

Gao, M. T. (2015). *Teaching Book of Seismic Zoning Map of China*. GB 18306–2015. Beijing: China Zhijian Publishing House. in Chinese.

Gardner, J. K., and Knopoff, L. (1974). Is the Sequence of Earthquakes in Southern California, with Aftershocks Removed, Poissonian? *Bull. Seismol. Soc. Am.* 64 (5), 1363–1367. doi:10.1785/BSSA0640051363

Ghazoui, Z., Bertrand, S., Vanneste, K., Yokoyama, Y., and Beek, P. (2019). Potentially Large post-1505 Ad Earthquakes in Western Nepal Revealed by a lake Sediment Record. *Nat. Commun.* 10 (1), 2258. doi:10.1038/s41467-019-10093-4

Gomez, B., Corral, Á., Orpin, A. R., Page, M. J., Pouderoux, H., and Upton, P. (2015). Lake Tutira Paleoseismic Record Confirms Random, Moderate to Major And/or Great Hawke's Bay (New Zealand) Earthquakes. *Geology* 43 (2), 103–106. doi:10.1130/G36006.1

Griffin, J. D., Stirling, M. W., and Wang, T. (2020). Periodicity and Clustering in the Long-Term Earthquake Record. *Geophys. Res. Lett.* 47, e2020GL089272. doi:10.1029/2020GL089272

Heki, K. (2003). Snow Load and Seasonal Variation of Earthquake Occurrence in Japan. *Earth Planet. Sci. Lett.* 207 (1-4), 159–164. doi:10.1016/S0012-821X(02)01148-2

Jiang, H., Mao, X., Xu, H., Yang, H., Ma, X., Zhong, N., et al. (2014). Provenance and Earthquake Signature of the Last Deglacial Xinmocun Lacustrine Sediments at Diexi, East Tibet. *Geomorphology* 204 (1), 518–531. doi:10.1016/j.geomorph.2013.08.032

Jiang, H., Zhong, N., Li, Y., Xu, H., Yang, H., and Peng, X. (2016). Soft Sediment Deformation Structures in the Lixian Lacustrine Sediments, Eastern Tibetan Plateau and Implications for Postglacial Seismic Activity. *Sediment. Geol.* 344, 123–134. doi:10.1016/j.sedgeo.2016.06.011

Jiang, H., Zhong, N., Li, Y., Ma, X., Xu, H., Shi, W., et al. (2017). A Continuous 13.3-ka Record of Seismogenic Dust Events in Lacustrine Sediments in the Eastern Tibetan Plateau. *Sci. Rep.* 7 (1), 15686. doi:10.1038/s41598-017-16027-8

Kagan, Y. Y., and Jackson, D. D. (1991). Long-term Earthquake Clustering. *Geophys. J. Int.* 104 (1), 117–134. doi:10.1111/j.1365-246X.1991.tb02498.x

Kirby, E., Reiners, P. W., Krol, M. A., Whipple, K. X., Hodges, K. V., Farley, K. A., et al. (2002). Late Cenozoic Evolution of the Eastern Margin of the Tibetan Plateau: Inferences from40Ar/39Ar and (U-Th)/He Thermochronology. *Tectonics* 21, 1. doi:10.1029/2000TC001246

Lei, J. C., Gao, M. T., and Yu, Y. X. (2007). Seismic Motion Attenuation Relations in Sichuan and Adjacent Areas. *Acta Seismol. Sin.* 29 (5), 500–511. in Chinese. doi:10.1007/s11589-007-0532-y

Li, G., West, A. J., Densmore, A. L., Jin, Z., Parker, R. N., and Hilton, R. G. (2014). Seismic Mountain Building: Landslides Associated with the 2008 Wenchuan Earthquake in the Context of a Generalized Model for Earthquake Volume Balance. *Geochem. Geophys. Geosyst.* 15 (4), 833–844. doi:10.1002/2013GC005067

Liang, L. J., and Jiang, H. C. (2017). Geochemical Composition of the Last Deglacial Lacustrine Sediments in East Tibet and Implications for Provenance, Weathering and Earthquake Events. *Quat. Int.* 430, 41–51. doi:10.1016/j.quaint.2015.07.037

Liu, Q., and Li, X. (2009). Preliminary Analysis of the Hanging wall Effect and Velocity Pulse of the 5.12 Wenchuan Earthquake. *Earthq. Eng. Eng. Vib.* 8 (2), 165–177. doi:10.1007/s11803-009-9043-2

Liu, M. (2014). *Research on the Risk Stone under Wind Loading with Wind Tunnel Test in the Min River Valley*. master thesis. Sichuan: Chengdu University of Technology, 1–95. in Chinese.

Lu, Y., Waldmann, N., Ian Alsop, G., and Marco, S. (2017). Interpreting Soft Sediment Deformation and Mass Transport Deposits as Seismites in the Dead Sea Depocenter. *J. Geophys. Res. Solid Earth* 122, 8305–8325. doi:10.1002/2017JB014342

Lu, Y., Wetzler, N., Waldmann, N., Agnon, A., and Marco, S. (2020). A 220,000-Year-Long Continuous Large Earthquake Record on a Slow-Slipping Plate Boundary. *Sci. Adv.* 6 (48), eaba4170. doi:10.1126/sciadv.aba4170

Moernaut, J., Daele, M. V., Heirman, K., Fontijn, K., Strasser, M., Pino, M., et al. (2014). Lacustrine Turbidites as a Tool for Quantitative Earthquake Reconstruction: New Evidence for a Variable Rupture Mode in South central Chile. *J. Geophys. Res. Solid Earth* 119 (3), 1607–1633. doi:10.1002/2013JB010738

Moernaut, J., Van Daele, M., Fontijn, K., Heirman, K., Kempf, P., Pino, M., et al. (2018). Larger Earthquakes Recur More Periodically: New Insights in the Megathrust Earthquake Cycle from Lacustrine Turbidite Records in South-central Chile. *Earth Planet. Sci. Lett.* 481, 9–19. doi:10.1016/j.epsl.2017.10.016

Moernaut, J. (2020). Time-Dependent Recurrence of strong Earthquake Shaking Near Plate Boundaries: a lake Sediment Perspective. *Earth-Sci. Rev.* 210, 103344. doi:10.1016/j.earscirev.2020.103344

Monecke, K., Anselmetti, F. S., Becker, A., Schnellmann, M., Sturm, M., and Giardini, D. (2006). Earthquake-induced Deformation Structures in lake Deposits: a Late Pleistocene to Holocene Paleoseismic Record for central Switzerland. *Eclogae Geol. Helv.* 99 (3), 343–362. doi:10.1007/s00015-006-1193-x

Montgomery-Brown, E. K., Shelly, D. R., and Hsieh, P. A. (2019). Snowmelt-triggered Earthquake Swarms at the Margin of long valley Caldera, California. *Geophys. Res. Lett.* 46, 3698–3705. doi:10.1029/2019GL082254

Oswald, P., Strasser, M., Hammerl, C., and Moernaut, J. (2021). Seismic Control of Large Prehistoric Rockslides in the Eastern Alps. *Nat. Commun.* 12 (1), 1059. doi:10.1038/s41467-021-21327-9

Owen, G., and Moretti, M. (2011). Identifying Triggers for Liquefaction-Induced Soft-Sediment Deformation in Sands. *Sediment. Geol.* 235 (3-4), 141–147. doi:10.1016/j.sedgeo.2010.10.003

Ran, Y. K., Chen, W. S., Xu, X. W., Chen, L. C., Hu, W., and Li, Y. B. (2014). Late Quaternary Paleoseismic Behavior and Rupture Segmentation of the Yingxiu-Beichuan Fault along the Longmen Shan Fault Zone, China. *Tectonics* 33 (11-12), 2218–2232. doi:10.1002/2014TC003649

Rodrı´guez-Pascua, M. A., Calvo, J. P., De Vicente, G., and Gómez-Gras, D. (2000). Soft-sediment Deformation Structures Interpreted as Seismites in Lacustrine Sediments of the Prebetic Zone, SE Spain, and Their Potential Use as Indicators of Earthquake Magnitudes during the Late Miocene. *Sediment. Geol.* 135 (1-4), 117–135. doi:10.1016/S0037-0738(00)00067-1

Sahu, B. K. (1964). Depositional Mechanisms from the Size Analysis of Clastic Sediments. *J. Sediment. Res.* 34, 73–83. doi:10.1306/74D70FCE-2B21-11D7-8648000102C1865D

Scharer, K. M., Biasi, G. P., Weldon, R. J., and Fumal, T. E. (2010). Quasi-periodic Recurrence of Large Earthquakes on the Southern San Andreas Fault. *Geology* 38 (6), 555–558. doi:10.1130/g30746.1

Shi, W., Jiang, H. C., Mao, X., and Xu, H. Y. (2020). Pollen Record of Climate Change During the Last Deglaciation from the Eastern Tibetan Plateau. *PLoS One* 15 (5), e0232803. doi:10.1371/journal.pone.0232803

Sims, J. D. (1975). Determining Earthquake Recurrence Intervals from Deformational Structures in Young Lacustrine Sediments. *Tectonophysics* 29 (1-4), 141–152. doi:10.1016/b978-0-444-41420-5.50020-4

Visini, F., and Pace, B. (2014). Insights on a Key Parameter of Earthquake Forecasting, the Coefficient of Variation of the Recurrence Time, Using a Simple Earthquake Simulator. *Seismol. Res. Lett.* 85 (3), 703–713. doi:10.1785/0220130165

Wei, X. T., Jiang, H. C., Xu, H. Y., Fan, J. W., Shi, W., Guo, Q. Q., et al. (2021). Response of Sedimentary and Pollen Records to the 1933 Diexi Earthquake on the Eastern Tibetan Plateau. *Ecol. Indicat.* 129, 107887. doi:10.1016/j.ecolind.2021.107887

Wen, X. Z., Zhang, P. Z., Du, F., and Long, F. (2009). The Background of Historical and Modern Seismic Activities of the Occurrence of the 2008 $M_s$ 8.0 Wenchuan, Sichuan, Earthquake2008. *Chin. J. Geophys.* 52 (2), 444–454. in Chinese.

Wesnousky, S. G. (1995). The Gutenberg - Richter or Characteristic Earthquake Distribution, Which Is it? *TransL. World Seismol.* 84 (6), 1940–1959. doi:10.1007/BF00807992

Wetzler, N., Marco, S., and Heifetz, E. (2010). Quantitative Analysis of Seismogenic Shear-Induced Turbulence in lake Sediments. *Geology* 38 (4), 303–306. doi:10.1130/G30685.1

Williams, R. T., Davis, J. R., and Goodwin, L. B. (2019). Do large Earthquakes Occur at Regular Intervals through Time? A Perspective from the Geologic Record. *Geophys. Res. Lett.* 46 (14), 8074–8081. doi:10.1029/2019GL083291

Woessner, J., and Wiemer, S. (2005). Assessing the Quality of Earthquake Catalogues: Estimating the Magnitude of Completeness and its Uncertainty. *Bull. Seismol. Soc. Am.* 95 (2), 684–698. doi:10.1785/0120040007

Worden, C. B., Gerstenberger, M. C., Rhoades, D. A., and Wald, D. J. (2012). Probabilistic Relationships between Ground-Motion Parameters and Modified Mercalli Intensity in California. *Bull. Seismol. Soc. Am.* 102 (1), 204–221. doi:10.1785/0120110156

Xu, H. Y., Jiang, H. C., Liu, K., and Zhong, N. (2020). Potential Pollen Evidence for the 1933 M7.5 Diexi Earthquake and Implications for Post-Seismic Landscape Recovery. *Environ. Res. Lett.* 15, 094043. doi:10.1088/1748-9326/ab9af6

Xu, H. Y., Jiang, H. C., Yu, S., Yang, H. L., and Chen, J. (2015). OSL and Pollen Concentrate $^{14}$C Dating of Dammed Lake Sediments at Maoxian, East Tibet, and Implications for Two Historical Earthquakes in AD 638 and 952. *Quat. Int.* 371, 290–299. doi:10.1016/j.quaint.2014.09.045

Xu, X., Wen, X., Yu, G., Chen, G., Klinger, Y., Hubbard, J., et al. (2009). Coseismic Reverse- and Oblique-Slip Surface Faulting Generated by the 2008 Mw 7.9 Wenchuan Earthquake, China. *Geology* 37 (6), 515–518. doi:10.1130/G25462A.1

Xu, C., Xu, X. W., Yao, X., and Dai, F. C. (2014). Three (Nearly) Complete Inventories of Landslides Triggered by the May 12, 2008 Wenchuan Mw 7.9 Earthquake of China and Their Spatial Distribution Statistical Analysis. *Landslides* 11 (3), 441–461. doi:10.1007/s10346-013-0404-6

Yang, N., and Zhang, Y. Q. (2010). Tission-track Dating for Activity of the Longmen Shan Fault Zone and Uplifting of the Western Sichuan Plateau. *J. Geomech.* 16 (4), 259–371. doi:10.1017/S0004972710001772

Yi, G. X., Wen, X. Z., Wang, S. W., Long, F., and Fan, J. (2006). Study on Fault Sliding Behaviors and strong-earthquake Risk of the Longmen Shan-Minshan Fault Zones from Current Seismicity Parameters. *Earthquake Res. China* 22 (2), 117–125. in Chinese. doi:10.3969/j.issn.1001-4683.2006.02.001

Yi, G. X., Wen, X. Z., and Su, Y. J. (2008). Study the Potential strong-earthquake Risk for the Eastern Boundary of the Sichuan-Yunnan Active Faulted-Block, China. *Chin. J. Geophys.* 56 (6), 1719–1725. in Chinese. doi:10.3321/j.issn:0001-5733.2008.06.012

Zhang, P. Z., Deng, Q. D., Zhang, M. G., Ma, J., Gan, W. J., Wei, M., et al. (2003). Active Tectonic Blocks and strong Earthquakes in the Continent of China. *Sci. China* 46 (2 Suppl. ment), 13–24. doi:10.1360/03dz0002

Zhang, P. Z., Xu, X. W., Wen, X. Z., and Ran, Y. K. (2008). Slip Rates and Recurrence Intervals of the Longmen Shan Active Fault Zone, and Tectonic Implications for the Mechanism of the May 12 Wenchuan Earthquake, 2008, Sichuan, China. *Chin. J. Geophys.* 51 (4), 1066–1073. in Chinese. doi:10.3321/j.issn:0001-5733.2008.04.015

Zhang, P. Z., Wen, X. Z., Shen, Z. K., and Chen, J. H. (2010). Oblique, High-Angle, Listric-Reverse Faulting and Associated Development of Strain: the Wenchuan Earthquake of May 12, 2008, Sichuan, China. *Annu. Rev. Earth Planet. Sci.* 38 (1), 353–382. doi:10.1146/annurev-earth-040809-152602

Zhang, P. Z. (2013). Beware of Slowly Slipping Faults. *Nat. Geosci.* 6 (5), 323–324. doi:10.1038/ngeo1811

Zhang, S. Q., Jiang, H. C., Fan, J. W., Xu, H. Y., Shi, W., Guo, Q. Q., et al. (2021). Accumulation of a Last Deglacial Gravel Layer at Diexi, Eastern Tibetan Plateau and its Possible Seismic Significance. *Front. Earth Sci.* 9, 797732. doi:10.3389/feart.2021.797732

Zhong, N., Jiang, H. C., Li, H. B., Xu, H. Y., Shi, W., Zhang, S. Q., et al. (2019). Last Deglacial Soft-Sediment Deformation at Shawan on the Eastern Tibetan Plateau and Implications for Deformation Processes and Seismic Magnitudes. *Acta Geol. Sin.* 93 (2), 430–450. doi:10.1111/1755-6724.13773

**Conflict of Interest:** The authors declare that the research was conducted in the absence of any commercial or financial relationships that could be construed as a potential conflict of interest.

**Publisher's Note:** All claims expressed in this article are solely those of the authors and do not necessarily represent those of their affiliated organizations, or those of the publisher, the editors and the reviewers. Any product that may be evaluated in this article, or claim that may be made by its manufacturer, is not guaranteed or endorsed by the publisher.